JACS
JOURNAL OF THE AMERICAN CHEMICAL SOCIETY

Article

pubs.acs.org/JACS

Two-Dimensional DNA-Programmable Assembly of Nanoparticles at Liquid Interfaces

Sunita Srivastava,[†] Dmytro Nykypanchuk,[†] Masafumi Fukuto,[‡] Jonathan D. Halverson,[†] Alexei V. Tkachenko,[†] Kevin G. Yager,[†] and Oleg Gang*[,†]

[†]Center for Functional Nanomaterials, Brookhaven National Laboratory, Upton, New York 11973, United States

[‡]Condensed Matter Physics and Materials Science Department, Brookhaven National Laboratory, Upton, New York 11973, United States

Supporting Information

ABSTRACT: DNA-driven assembly of nanoscale objects has emerged as a powerful platform for the creation of materials by design via self-assembly. Recent years have seen much progress in the experimental realization of this approach for three-dimensional systems. In contrast, two-dimensional (2D) programmable nanoparticle (NP) systems are not well explored, in part due to the difficulties in creating such systems. Here we demonstrate the use of charged liquid interfaces for the assembly and reorganization of 2D systems of DNA-coated NPs. The absorption of DNA-coated NPs to the surface is controlled by the interaction between a positively charged lipid layer and the negatively charged DNA shells of particles. At the same time, interparticle interactions are switchable, from electrostatic repulsion between DNA shells to attraction driven by DNA complementarity, by increasing ionic strength. Using in situ surface X-ray scattering methods and ex situ electron microscopy, we reveal the corresponding structural transformation of the NP monolayer, from a hexagonally ordered 2D lattice to string-like clusters and finally to a weakly ordered network of DNA cross-linked particles. Moreover, we demonstrate that the ability to regulate 2D morphology yields control of the interfacial rheological properties of the NP membrane: from viscous to elastic. Theoretical modeling suggests that the structural adaptivity of interparticle DNA linkages plays a crucial role in the observed 2D transformation of DNA-NP systems at liquid interfaces.

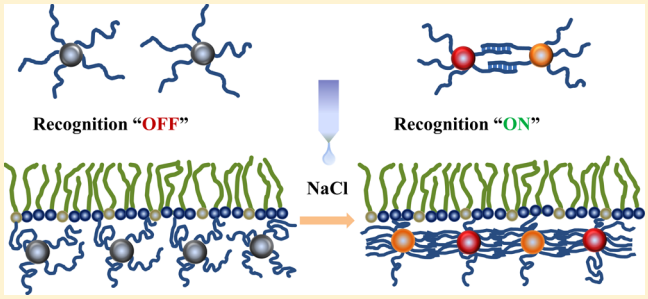

INTRODUCTION

Structural organization of molecules at liquid interfaces gives rise to rich behavior in soft matter systems. For instance, surface molecules induce bulk ordering in liquid crystals,[1,2] exhibit extraordinary freezing effects,[3,4] and form diverse phases.[5−8] One of the central structural constituents of living matter, the cell membrane,[9] is organized by Nature around interfaces of amphiphilic molecules. The fluidity of liquid interfaces, in contrast to solid surfaces, provides favorable conditions for mass transport and chemical reactions,[10] and it allows for structural responsiveness.[11,12] These attractive properties of liquid interfaces were recently exploited for nanoscale objects, leading to the formation of shaped droplets,[13] optically active layers,[14,15] and films with remarkable mechanical and filtration properties.[16,17] One of the outstanding difficulties in the organization of nanoscale systems at liquid interfaces is the limited ability to regulate surface−particle and particle−particle interactions. For molecular systems, these interactions are often balanced by the tuning of hydrophobic and hydrophilic molecular parts. This approach is difficult to realize controllably for nanoscale objects. In this study we explore how to exploit the sequence-specific programmability of DNA binding and DNA polyelectrolyte properties for the formation of nanoparticle (NP) membranes at liquid interfaces. As we show below, such systems exhibit a peculiar two-dimensional (2D) phase transformation due to the novel interplay of interplay of programmable binding with chain and colloidal effects.

Recent progress in DNA-mediated particle assembly demonstrates that the selectivity of Watson−Crick binding can be successfully utilized for creating 3D superlattices,[18,19] heterogeneous assemblies,[20,21] surface-promoted particle layers,[22,23] and linear mesostructures.[24] In this work we demonstrate a framework for assembly and tuning of 2D DNA-based NP systems at liquid interfaces, which enables the creation of programmable membrane morphologies from NPs. We control the particle−surface and particle−particle interactions, which are reminiscent of hydrophobic/hydrophilic effects in molecular systems, using the liquid−vapor interface with a charged lipid layer[25] and DNA shells, respectively. The interactions are tuned via salt concentration, from a regime dominated by interparticle electrostatic repulsion of DNA chains to a regime of strong attraction due to DNA

Received: February 19, 2014
Published: May 6, 2014

   dx.doi.org/10.1021/ja501749b | J. Am. Chem. Soc. 2014, 136, 8323−8332

hybridization. Using a range of in situ surface X-ray scattering methods and ex situ electron microscopy, we reveal different structural organizations of this 2D NP "skin". Observed morphological transformations are directly coupled with changes in the interface viscoelastic behavior. The mechanism of this multistage transformation is also studied by complementary theoretical investigations.

RESULTS

The experimental design for programmable assembly of DNA-functionalized nanoparticles (DNA-NPs) in two dimensions at lipid-coated air−water interfaces is shown in Figure 1. The

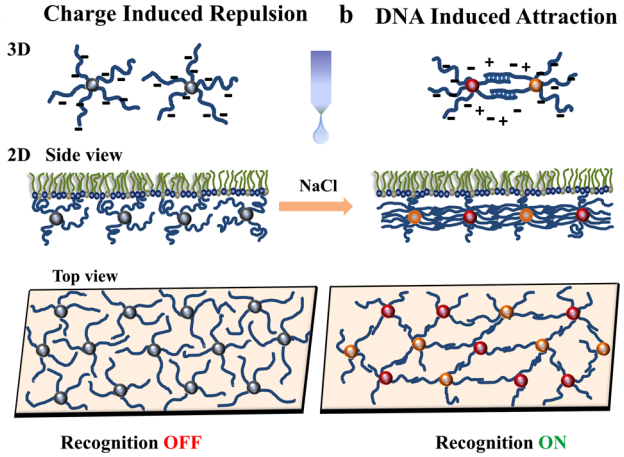

Figure 1. Schematic illustration of the assembly of DNA-functionalized NPs at positively charged interfaces. (a) In the absence of salt, interactions are dominated by the electrostatic repulsion between DNA chains. (b) The 2D assemblies can be altered by programming the interactions between the NPs. By introducing monovalent salt, an attractive interaction between the NPs is switched ON, due to DNA hybridization. Change in interaction between NPs provides the path to tune the structure of the 2D assemblies at the interface.

electrostatic attraction between negatively charged DNA-NPs and the positively charged lipid interface facilitates the adsorption and formation of a DNA-NP monolayer at the interface. To probe the effect of surface charge on the 2D assemblies, we investigated lipid monolayers with two different mixtures of the cationic 1,2-dimyristoyl-3-trimethylammonium-propane (DMTAP) and neutral 1,2-dimyristoyl-*sn*-glycero-3-phosphocholine (DMPC)[25] lipids (see Materials and Methods and Supporting Information (SI) for details). The monolayers with 1:0 and 1:1 compositions of DMTAP:DMPC lipids are defined as S_{strong} and S_{weak}, respectively. System S_{strong} has stronger electrostatic affinity between the lipid and NP layer as compared to system S_{weak}, due to higher interfacial charge. Subsequently, solution containing an equimolar mixture of two types of gold NPs, where each type of particle is functionalized with ssDNAs (50 bases) and ssDNAs from both particles are complementary, is introduced into the bulk subphase containing salt-free water.

In the absence of salt in the subphase, complementary particles are attracted to the surface but are not able to hybridize (Figure 1a, hybridization is OFF). Under these conditions, NPs experience mutual repulsion due to their negatively charged DNA coronas and steric interactions of the chains. A 2D arrangement of NPs forms within 10−15 min after particles are injected (this is a minimum time required to probe the interface with in situ X-ray scattering). Accordingly, mutual interparticle repulsion, combined with particle attraction to the interface, determines the in-plane structure of the NP monolayer.[26] Under zero salt conditions, the specificity of DNA encoding is irrelevant since DNA hybridization cannot occur and the particles coated with complementary DNA sequences are effectively indistinguishable. By adding a small amount of salt, an attractive interparticle interaction is switched ON due to the sequence-specific Watson−Crick base-pairing of complementary ssDNA (Figure 1b), and interparticle linkages are established via the formation of hybridization bridges. To monitor the in situ structure of the NP assembly at the interface, we used a combination of synchrotron surface scattering techniques, grazing-incidence small-angle X-ray scattering (GISAXS), and X-ray reflectivity (XRR), which correspondingly provide information on in-plane and surface-normal monolayer structure. Structural ordering was confirmed via complementary ex situ scanning electron microscopy (SEM) of the NP assemblies transferred to a solid support. The viscoelastic properties of the monolayer were investigated using interfacial rheology.

At 0 mM NaCl, the addition of an equimolar mixture of complementary DNA-functionalized NPs to the water subphase results in the formation of an ordered NP monolayer at the air−liquid interface, as evident from the GISAXS pattern for system S_{strong} (Figure 2a). The analysis of peak positions in the structure factor $S(q_r)$ (obtained as $S(q_r) = I(q_r)/F(q_r)$, where $F(q_r)$ is the particle form factor measured for the dispersed NPs in solution and q_r is the in-plane scattering wave vector) reveals $q_i/q_{10} \approx 1{:}\sqrt{3}{:}\sqrt{4}{:}\sqrt{7}{:}\sqrt{9}...$ (i is the peak index). Such a diffraction pattern signifies a 2D hexagonal structure, as shown in Figure 2a, with corresponding diffraction from (10), (11), (20), (21), and higher-order lines. This hexagonal structure was observed for DNA-coated particles at free air−liquid interfaces.[27] The GISAXS pattern in Figure 2a exhibits 10 orders of diffraction peaks, demonstrating a remarkable degree of long-range ordering in the self-assembled NP monolayer. The observed rod-like intensity distribution indicates the assembly is 2D. The surface potential for adsorption of NPs at the liquid interface is determined by the lipid charge density. The higher composition of cationic lipid results in an increase of the surface potential, 540 mV for S_{strong} vs 500 mV for S_{weak} (at ∼0 mM salt), estimated using the Grahame equation (Figure S5).[28] Therefore, it is not surprising that slightly weaker ordering was observed (Figures S3 and S4) for S_{weak}, which has a lower cationic lipid content. However, we found that the type of crystalline structure remains the same (hexagonal close packing, HCP), as confirmed by seven diffraction peaks (Figure S3).

An increase of salt concentration in the subphase to 5 mM dramatically changes the interactions in the system: the onset of Watson−Crick recognition between complementary DNA chains provides attraction, and electrostatic repulsion between negatively charged DNA shells is significantly screened, whereas the steric repulsion remains between particles of the same kind. The activation of specific interactions effectively transforms the system from a quasi-single-component system, where particles are indistinguishable, to a two-component state (as defined by DNA shells). This reversal of interactions causes the transition of the HCP lattice to isolated string-like clusters, as revealed by GISAXS measurements (Figure 2b) and by SEM as discussed below. The relative peak positions in $S(q_r)$ at 5 mM are $q_i/q_1 \approx$ 1:2:3:4, which in 2D is consistent with a linear arrangement of equally spaced particles. We performed control measurements

dx.doi.org/10.1021/ja501749b | J. Am. Chem. Soc. 2014, 136, 8323−8332

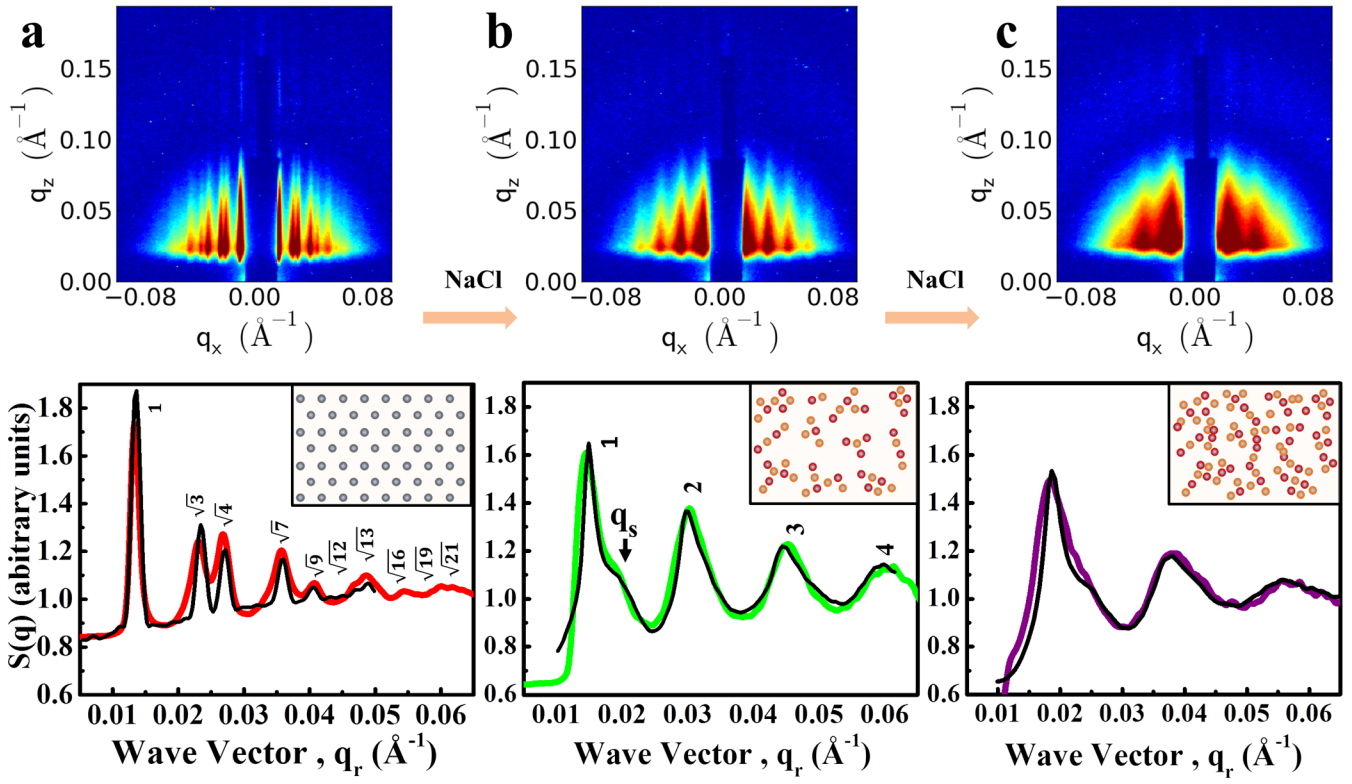

Figure 2. In situ GISAXS images (q_z and q_r represent the surface-normal and in-plane components of the scattering wave vector, respectively) of nanoparticle layers at different salt concentrations (top), along with the extracted structure factor $S(q_r)$ profiles (bottom). (a) At 0 mM NaCl, peak position ratios in (q_i/q_1) indicate that NPs are arranged in a 2D hexagonal lattice. (b) At 5 mM NaCl, linkage between DNA chains via hybridization induces a phase transition to a string-like cluster morphology of connected NPs. (c) At ∼50 mM, DNA linkages between particles result in the formation of a percolated weakly ordered NP monolayer. Cartoons in the bottom insets represent the morphology of particle assemblies used in the X-ray simulations to fit data (black solid line) for HCP, cluster, and connected cluster phases, respectively.

using a sample containing NPs functionalized with only one type of ssDNA (50 bases) (in situ GISAXS, Figure S1, and ex situ SEM, Figure S3). These particles, with noncomplementary DNA coatings, are not expected to exhibit DNA-induced bonding. For this control sample we observe an HCP phase at zero salt, as in the case of complementary particles. However, unlike the systems of complementary particles, which shows a structural transition with salt addition, the HCP phase of the single-type NP system remains and does not exhibit any transformation, even when the salt concentration is increased to 5 mM NaCl. Thus, we conclude that switching ON of DNA recognition between NPs for both S_{weak} and S_{strong} leads to the formation of the string/cluster morphology through the formation of interparticle connections via hybridization of DNA chains. Interestingly, the onset of the hybridization-induced phase transition at the interface occurs immediately (within 10−15 min) at the subphase salt concentration of 5 mM. The rapid assembly at such low salt concentration for this 2D system vs a 3D DNA-NP assembly (∼3 days) may be attributed to the electrostatic formation of the particle layer, in which NP and DNA concentrations are significantly higher than in the bulk.

To assess the structure of the particle monolayer quantitatively, we modeled the GISAXS profiles for our system with "recognition OFF" (dominance of electrostatic interactions) and "recognition ON" (dominance of Watson−Crick interactions) states, and we then compared the calculated and observed structure factors. Our modeling of the scattering data shows that the system with recognition ON is well-described by string-like particles clusters (Figure S12). We found that occasional additional particles bonded at 90° relative to the axis of the main chain are necessary to capture the shoulder peak at $q_s/q_1 \approx 1.4$. Such a morphology can be viewed as string-like structure with random branching, as indicated in Figure 2b (details of the data modeling and snapshots cluster populations are given in Figure S12). The string-like character of clusters formed by the hybridized particles is also observed for S_{weak} (Figure S3). Moreover, in this case, we do not observe the shoulder peak, signifying limited branching, which is possibly due to the higher mobility of particles at the lipid interface with lower surface charge density (see the rheology results below). With an increase in subphase salt concentrations, at or above 50 mM (Figure 2c), the correlation length is significantly reduced, and the monolayer can be modeled as a disordered phase consisting of random disordered branched structures.

The GISAXS study of the structural development of the NP membrane with increasing ionic strength reveals a gradual change of interparticle distance, H, as shown in Figure 3a. At 0 mM, the in-plane particle−particle separation for the HCP lattice, H_{hcp}, is obtained from

$$\left\{\frac{4\pi}{\sqrt{3}}\frac{1}{q_{10}} - 8.5\right\}\text{nm}$$

where q_1 is the position of the first diffraction peak in the in-plane scattering line profiles and 8.5 nm is the diameter of the NP gold core. The strong electrostatic attraction with the positively charged lipid surface for system S_{strong} results in the

dx.doi.org/10.1021/ja501749b | J. Am. Chem. Soc. 2014, 136, 8323−8332

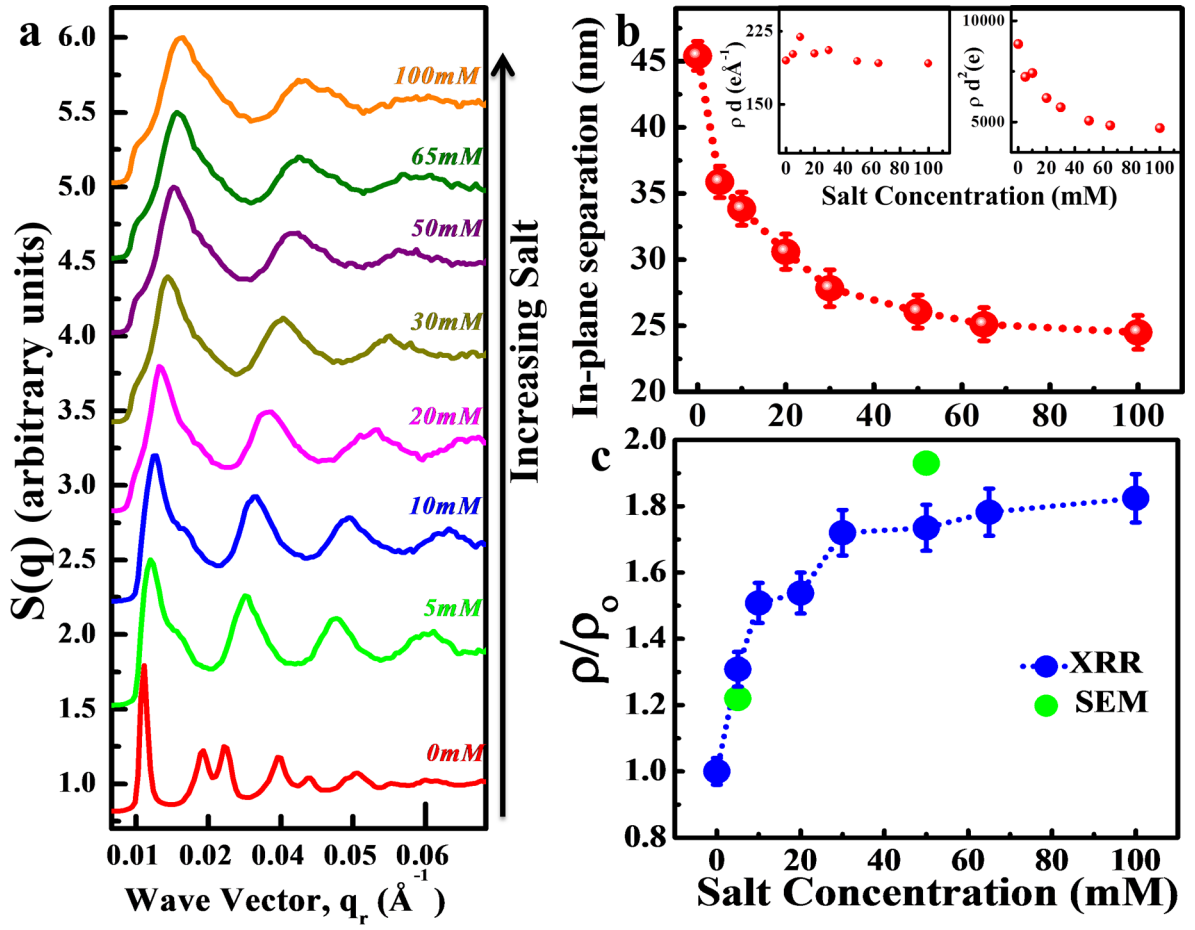

Figure 3. In-plane (GISAXS) structure of the 2D NP assemblies. (a) The $S(q_r)$ profiles extracted from the GISAXS images at different salt concentrations (shifted vertically for clarity). (b) The in-plane particle−particle separation, H (H_{hcp} at 0 mM and H_{str} for >0 mM), as a function of a salt concentration. Dotted lines connecting symbols are to guide the eye. Inset: Product of ρ (surface density obtained from XRR) and d or d^2 (where d is the in-plane center-to-center distance measured from GISAXS). (c) Bulk-normalized relative surface density (ρ/ρ_0) of the NP layer measured by XRR (in situ) and estimated from SEM (ex situ) data. XRR data were fit (SI) using Motofit package in Igor Pro.

increased adsorption of NPs, and the measured H_{hcp} = 45.6 nm is smaller than the 50.1 nm distance measured for S_{weak} (SI). For the string-like cluster phase for S_{strong}, the corresponding separation $H_{str} = (2\pi/q_{10} - 8.5)$ nm decreases from 35 to 24 nm as the salt concentration increases to 100 mM (Figure 3b). The broadening of scattering peaks (Figure 3a and Figure S4) at high salt concentration indicates a degradation of the in-plane order, possibly due to the higher degree of branching and reduced bond orientational order. These changes are accompanied by a decrease in the DNA persistence length, as evident from the reduction of H_{str} at those salt concentrations. This shrinking of the NP coronas, in turn, results in an increase of the available surface area, allowing additional NPs to adsorb to the lipid interface. We note that our measurements do not have a signature of 3D growth of NP clusters (GISAXS, Figures 2 and 3; XRR, Figure S7) from the interface and into the subphase. Indeed, the first layer of adsorbed particles benefits from electrostatic attraction to the interface, while subsequent layers would only form due to weaker hybridization. However, the larger number of available bonds in bulk 3D aggregation, as well as the reduced surface energy in this case, favors the formation of a purely 2D NP layer.

Direct evidence of 2D assembly was obtained by probing the surface-normal structure of the NP monolayer as a function of salt concentration with XRR (Figure S7a). Complementary optical microscopy studies (Figure S8) indicate that the monolayers are homogeneous at the scale of a few micrometers and larger, which validates the use of XRR modeling with a single electron-density (e-density) profile. We applied the Parratt formalism[29] to fit the XRR data with a box model (using Motofit package in Igor Pro[30]) to obtain e-density profiles of the NPs at the lipid interface (see SI and Figure S7b). We show in Figure 3c the change of the relative surface e-density of the gold NP layer ρ/ρ_0, as obtained from the XRR analysis; here ρ is defined as the integration of the excess of e-density over the lipid layer at a given salt concentration. At 0 mM, ρ is denoted as ρ_0. The ρ/ρ_0 increases by a factor of about 1.8, which qualitatively agrees with the interparticle distance decrease determined by GISAXS. Comparable changes were observed in the ex situ SEM measurements for the monolayers transferred to the solid support (Figure 3c), as estimated from the number of particles per area. The character of surface morphology can be estimated from the ρd^{α} behavior, where α = 1 and 2 correspond to 1D and 2D structures, respectively, and the interparticle spacing $d = H + 8.5$ nm depends on the salt concentration. The inset of Figure 3b demonstrates that ρd^2 shows a significant decrease and ρd is nearly constant, suggesting a linear growth of branched rigid structures with increase in salt concentration. This observation is in line with GISAXS analysis suggesting a string-like character of 2D

dx.doi.org/10.1021/ja501749b | J. Am. Chem. Soc. 2014, 136, 8323−8332

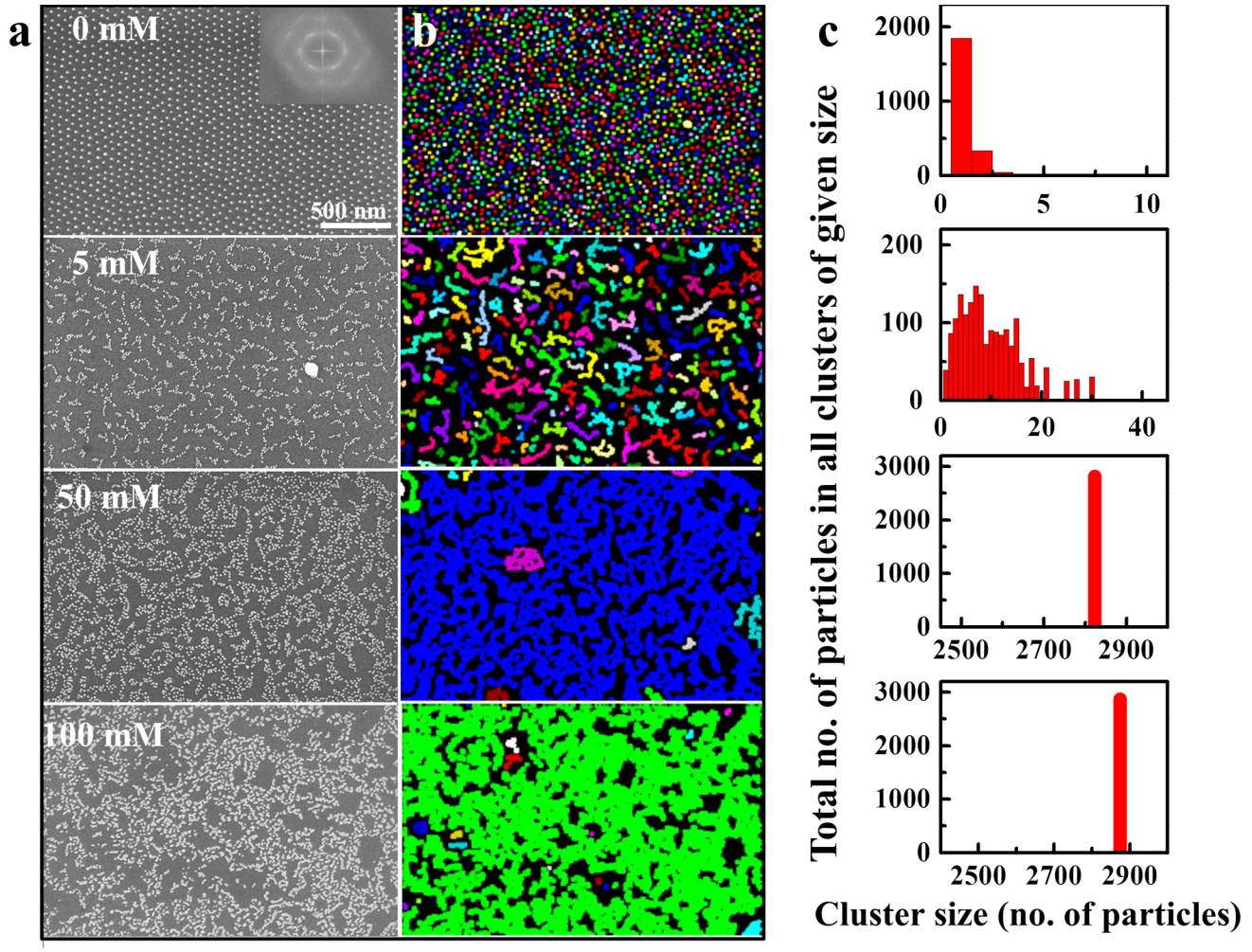

Figure 4. (a) SEM images of dried NP layers transferred from a liquid surface onto positively charged substrates at the labeled salt concentrations. The scale bar is the same for all images. The Fourier transform of the SEM image at 0 mM (inset) clearly indicates hexagonal packing of NPs. (b) False color image of the SEM data shown in (a) to quantify the number of NPs in strings/clusters (particles in the same cluster are colored the same). (c) Analysis of SEM images quantifying the connectivity of particle assemblies, as a function of salt concentration. The abscissa is the size of clusters in terms of the number of particles per cluster and the ordinate is the total number of particles present in all cluster of a given size. The size of the cluster grows with addition of salt, and almost all particles are interconnected in a network at 50 and 100 mM.

assemblies with added salt (>0 mM NaCl) rather than a uniform 2D layer. Thus, the applied X-ray scattering methods reveal that, by varying the salt concentration, the 2D hexagonal lattice of mutually repulsive particles at 0 mM undergoes a transition to a DNA-linked morphology dominated by string-like particle clusters in the intermediate salt regime (<50 mM), which eventually become a 2D amorphous structure at higher salt concentrations (≥50 mM). This is accompanied by a decrease in the corresponding particle−particle separation from about 45 to 24 nm (Figure 3b). The real-space structure of the NP layer was also examined by ex situ SEM. The NP layers at different subphase salt concentrations were transferred to positively charged silicon substrates (SI), which allows immobilizing the assembled morphology in a state close to the one at the water interface. We show representative SEM images of the transferred NP layers in Figure 4a. A hexagonal lattice (Figure 4a, left top) with excellent order, as confirmed by the Fourier transform (inset), was observed at 0 mM. The transition to a structure with NPs arranged in a predominantly linear manner—yet only forming clusters—is observed at 5 mM. The SEM image for the control sample at 5 mM shows that the hexagonal morphology (Figure S2) is preserved for one-type NP systems.

The subsequent salt increase for system with complementary NPs results in a transition to a fully percolated 2D structure at high salt concentration (≥50 mM, see Figure 4). The detailed image analysis of SEM data, showing maps of connected NPs, is shown in Figure 4b. Particles identified as locally connected are shown using the same color. Since the DNA chains are not visible in the SEM images, we used threshold value of ∼35 nm, based on estimates of particle−particle bonding distances, as a criterion to establish connectivity between neighboring particles. The corresponding histograms of 2D cluster size are shown in Figure 4c. The hexagonal phase is dominated by well-separated particles. As soon as DNA hybridization occurs (5 mM salt), string-like clusters form with up to ∼20 particles per cluster. Subsequently, at 50 mM and above, the nanoclusters form a network, in which all particles constitute one single aggregate occupying the whole frame, about 3000 particles (limited by the field of view of a few micrometers). Only a few small clusters can still be observed at this stage. Thus, both X-ray scattering and SEM imaging demonstrate that the NP system undergoes a transition from a well-defined HCP lattice

dx.doi.org/10.1021/ja501749b | J. Am. Chem. Soc. 2014, 136, 8323−8332

to string-like morphologies when hybridization occurs. Moreover, imaging reveals the topological rearrangement of NPs when the recognition is already ON: isolated string-like nanoclusters transform into a network of particles connected by DNA chains (not visible on SEM images).

Direct evidence of this topological transformation, from disconnected clusters to extended network, was obtained from in situ measurements of the macroscopic mechanical properties of the NP monolayer, using interface rheometry.[31] We probed the shear modulus of the monolayer in the recognition OFF and recognition ON states of the system at different salt concentrations, using time-sweep and oscillatory-frequency-sweep measurements. To ensure the linear response of the NP monolayer, an optimal strain of 2% was identified through amplitude sweep measurements, for which the moduli were measured with increasing strain at fixed oscillatory frequency of 1 Hz. All frequency sweep measurements were done at this strain. For time sweep measurement of the viscous samples, optimal strain was used to get good signal-to-noise ratio.

To compare the in situ changes of the rheological response (elastic and storage moduli are G' and G'', respectively) with the corresponding observed structural transformations, we show the time sweep data for S_{strong} and S_{weak} in Figure 5. Our

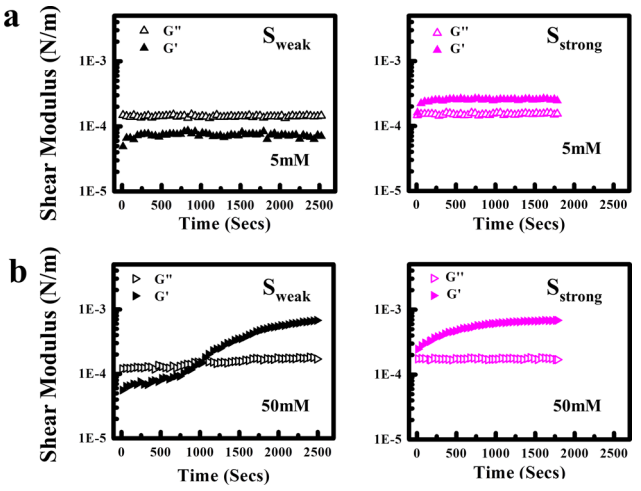

Figure 5. Time-sweep data obtained from rheological measurements (at oscillatory frequency of 1 Hz), after addition of (a) low salt (5 mM) and (b) high salt (50 mM) for S_{weak} (left) and S_{strong} (right) systems. After addition of 50 mM salt (t = 0 s), both systems exhibit structure-dependent responses. The shear elastic modulus (G', closed symbols) and storage modulus (G'', open symbols) are as indicated alongside each graph.

measurements reveal the differences between the transient (0–20 min after salt addition) and steady state (>20 min) rheological behaviors of both systems at low (<5 mM) and high (>50 mM) salt concentrations. We observed that at low salt, the systems S_{strong} and S_{weak} exhibit a time-independent rheological response. The elastic shear modulus for S_{strong} is higher than S_{weak}, suggesting the NP assembly is more elastic. At high salt, for S_{weak} the viscous response dominates the elastic response ($G'' > G'$), before and immediately after adding salt. With time, a percolated network forms and G' increases significantly, exceeding G'' for both systems, which manifest an elastic response of the NP monolayer.

These measurements allow assessing the influence of the lipid layer composition on the rheological properties of the lipid-NP interface. At low salt (Figure 5a), G'' was found to be consistently greater than G' for S_{weak}, whereas the opposite, $G' > G''$, was observed for S_{strong}. Such higher elastic properties of S_{strong} can be attributed to a stronger electrostatic interaction between the NPs and the lipid layer. At high salt (Figure 5b), before and immediately after salt addition, the NP monolayer for S_{weak} shows liquid-like behavior with $G' < G''$. With time, as the number of DNA linkages between NPs in the monolayer increases and a network forms, a crossover to more solid-like monolayer, with $G' > G''$, is observed, after about 1000 s. Similarly, G' for S_{strong} also grows with time. The time sweep rheology measurement for the control sample (NPs functionalized with only one type of DNA) does not show any increase in G' with salt addition. In fact, the magnitude of G' decreases with salt increase due to softer (reduced persistence length) nonlinked DNA coronas (Figure S10). Thus, the increased interparticle connectivity through DNA hybridization is the driving force for observed transition to an elastic monolayer for S_{weak} and S_{strong} systems, as evident from our rheological measurements. In order to investigate the effect of the interaction of the NP layer with the surface and to identify the rheological phase of the monolayer, we performed frequency sweep measurements, as shown in Figure 6. At low salt, both systems exhibit frequency-dependent response. For S_{weak} at 0 mM salt, the elastic modulus G' is small (within the detection limit of the instrument). The shear modulus, $G'' > G'$, indicates a fluid-like monolayer and, therefore, the data for G' have large error bars (Figure 6a). For S_{strong} at low salt (0 and 5 mM), the shear modulus exhibits a frequency dependence, suggesting the formation of a viscoelastic monolayer with partial and imperfect cross-linking. The power-law exponents for the frequency dependence of the elastic moduli, at low salt, for S_{strong} and S_{weak} are 0.2 and 0.8, respectively. At high salt concentrations (50 and 100 mM), both systems yield an exponent of ~0 (Figure 6a), as expected for a perfect cross-linked network. The 3D analogue of such a network demonstrates remarkable compression properties which are determined by the molecular details of the connecting DNA linkages.[32]

In Figure 6b we summarize our findings on probing mechanical properties of DNA-programmable NP monolayers. The three different rheological responses, such as viscous, viscoelastic and elastic, were observed for both systems (S_{strong} and S_{weak}) and can be attributed to the formation of DNA-linked NP morphologies at different salt concentrations. Although the strength of the electrostatic interaction between the NPs and the lipid layer are tuned by the composition of the cationic lipid (shift of rheological response from viscous to viscoelastic regime), the major changes occur when a fully interconnected 2D network is formed (elastic monolayer).

■ DISCUSSION

The origin of the observed structural and rheological transition lies in the interplay of electrostatic and DNA-driven interactions, and in the 2D character of the system. One could expect that analogously to three-dimensional systems of complementary particles of similar sizes—for which the ground state is a BCC phase[18,19]—a square lattice would most likely be the equilibrium phase for the present 2D system. In contrast to the 3D case, where a BCC phase of particles form by aggregation from the "gas" phase, the initial state (no salt) for the 2D system is liquid-like, electrostatically stabilized by the interparticle repulsion and particle–lipid interface attraction.

dx.doi.org/10.1021/ja501749b | J. Am. Chem. Soc. 2014, 136, 8323–8332

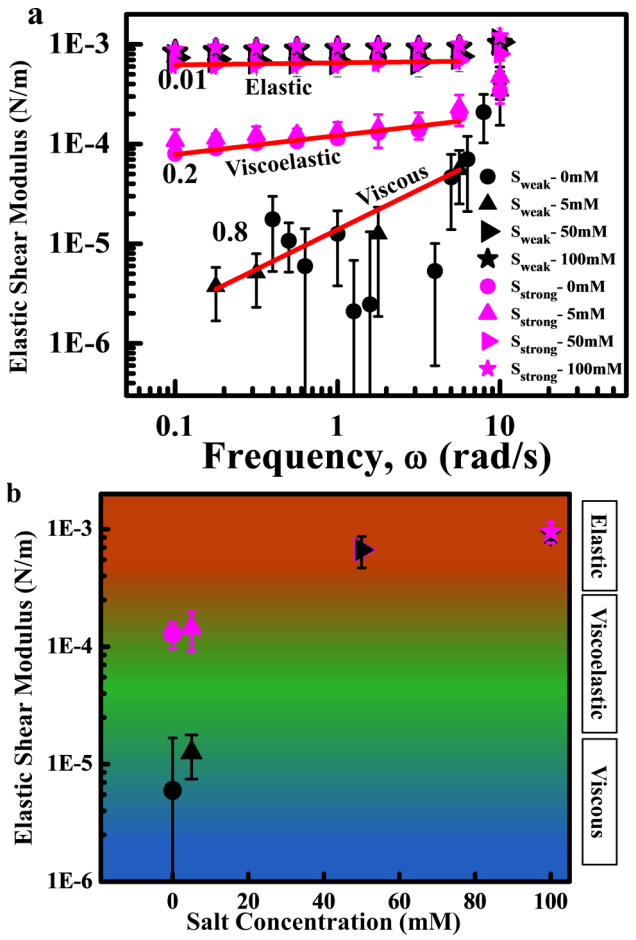

Figure 6. (a) Frequency sweep data showing elastic shear modulus, G', vs angular frequency, ω. Transitions in the rheological behavior of a monolayer, from viscous to viscoelastic and to elastic, were observed by varying the composition of the lipid layer, and salt concentration: ●, 0; ▲, 5; ▶, 50; and ★, 100 mM. Black color denotes S_{weak} and magenta denotes S_{strong}. For S_{weak}, at 0 and 5 mM, the monolayer is viscous and the elastic shear modulus (G') is within the measurement limit of the instrument, as is evident from the large error bars in the data. (b) Comprehensive plot of G' vs salt concentration for both systems, S_{strong} and S_{weak}, showing the different rheological phases observed for 2D DNA-NP monolayer. Symbols are the same as in part a.

The onset of recognition between NPs with complementary DNA types drastically affects in-plane interactions. The 2D NP layer is adhered to the lipid surface through strong electrostatic attraction, preventing any in-plane reorganization of NPs. Moreover, the experimental systems are always below their DNA-hybridization melting temperatures (Figure S6), ensuring effective irreversibility of the DNA connections at any given salt concentration. In order to transform continuously into a square lattice from the random distribution of particle types in the original hexagonal lattice, the rearrangement of particles requires their global movement and therefore the system naturally finds itself in a frustrated state.

In principle, the observed transition of the NP system from a repulsive crystal to a weakly ordered network via linear clustering can be rationalized by considering generic interparticle interaction potentials that can be tuned from nonspecific repulsion to specific, particle-type-dependent attraction. However, as one might intuitively expect, switching ON such attraction would result in an abrupt and complete aggregation of the system.[33] This is not consistent with the scenario observed experimentally. The most puzzling part of the observed behavior is the formation of finite-size clusters with distinct string-like morphology. One of the general scenarios for the formation of string/stripe like structures for particles in confinement is related to the competition between short-range attractive and long-range repulsive interactions[34−37] or different scales of repulsions.[38,39] By contrast, our system shows a unique scenario where a string-like morphology appears. Here DNA hybridization is a major interaction factor and the repulsion range is significantly smaller than the particle size. Indeed, even at the lowest salt concentrations the screening length is only a few nanometers.

In order to understand the system behavior, in particular the transition from the hexagonal lattice to string-like cluster assemblies, we conducted Monte Carlo (MC) simulations[40] for the model 2D system of particles (SI). At initialization, the particles were assigned to the fixed sites of a periodic triangular lattice, similar to the experimental findings, with the H_{hcp} = 45.6 nm. The particles of complementary types were assigned randomly to the lattice sites confined in a 2D plane (to mimic the interaction with the lipid layer), with the final overall composition of each type being 1/2. Particles interacted via a repulsive potential whose strength decreased with increasing salt concentration. A stochastic scheme was used to create irreversible bonds representing DNA hybridization between particles with increased salt. Since the average bond length is less than the initial interparticle spacing, as the particles assemble, free space is created. New particles were added in simulations to mimic the experimental conditions for which we measured increase in the density of NPs at the surface. For the simulations, the average bond length was taken from the experimental data and particle insertion MC moves were used to capture the NP adsorption behavior. This model allows us to observe the transition from a triangular lattice to a percolating network (Figure 7a, high salt); however, no finite string-like morphologies were observed. Hence, to describe the experimental findings, some additional factors are necessary; in particularly, to account for the effect of DNA chains in a particle shell.

Recent studies show that multiple DNAs hybridizing between particles can lead to a number of collective chain effects, e.g., spontaneous breaking of symmetric interactions[24] and interparticle bond shortening were reported.[41] The origin of these effects lies in the ability of relatively long (comparable to a particle diameter or larger) chains from the shell to adopt conformations which will maximize the number of bridges between particles. We include this effect in our model as follows: particles should only form bonds at angles above a certain threshold value which is larger than that suggested by the purely geometrical consideration of particle shape. Consider two particles with short DNA chains. In this case a DNA participating in the bond between the particles is located at the point of particles contact. A third particle can bind at any angle θ permitted by the geometrical considerations; e.g., for particles of same sizes, minimum $\theta > 60°$. On the other hand, for particles with longer DNA chains, the chains located far from the point of contact, for example on the particle sides, can reach over and participate in the bonding. This means that when a second bond (with a third particle) is formed, it will tend to be at a large angle relative to the first bond. We account for this effect in our model by assuming that a second bond can only

dx.doi.org/10.1021/ja501749b | J. Am. Chem. Soc. 2014, 136, 8323−8332

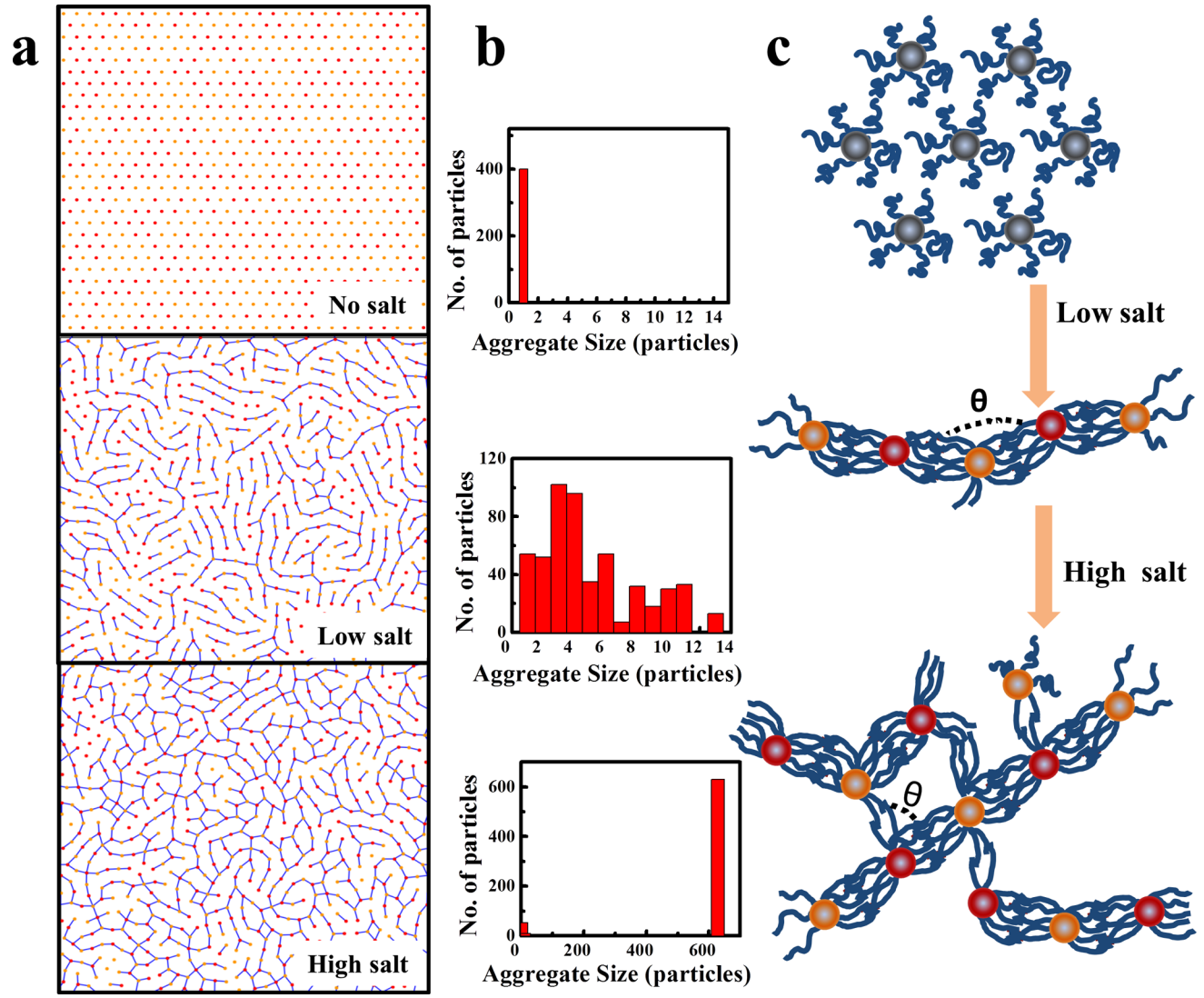

Figure 7. Computational results. (a) Top: At initialization the two particle types, corresponding to NP with complementary DNA, are randomly assigned to the sites of a triangular lattice. Center: At an intermediate salt concentration, the angle between NP bonds, θ, is 135°, and the particles are found to self-assemble into string-like structures (see also text), as shown in center part of (c). Bottom: A percolating network is found at high salt concentration when θ = 90° or lower. (b) Alongside each graph are shown the statistics of the aggregate size. The histograms show the distribution of aggregate size; to be compared with experimental observations in Figure 4c. (c) Cartoons represent the mechanism for phase transition from HCP to string-like morphology and to the NP network: (top) nonhybridizing DNA-coated NPs stabilize into an HCP lattice due DNA shell repulsion at 0 mM; (center) a linear morphology is promoted at low salt when the number of sequence-specific DNA linkages between two particles is maximized; (bottom) due to the reduced persistence length of DNA chains and their increased entropy, not all those linkages can survive at the higher salt, which results in increased connectivity with other complementary particles, and the formation of a network (see text for details).

form if the resulting angle is larger than θ as defined in Figure 7b. We refer to this concept as the principle of competing binding, which is analogous to the formation of linear ribbons for nanorods in 3D assembly.[24] The simulations were repeated applying this concept; and indeed string-like assemblies were observed when the limiting bond angle θ is about 135°, as shown in Figure 7a (low salt). At higher salt concentrations (50 mM), the persistence length of ssDNA decreases considerably,[42] resulting in reduced chain extension and increased chain entropy. Consequently, hybridizations for the less extended chain located far from the point of particle−particle contact is suppressed, which results in the reduction of θ. Our simulations show that population of clusters with network structure appear when θ decreases below 135°. A fully percolating network, analogous to the experimentally observed structure at high salt concentration, was found at θ = 90° (Figure 7a).

Thus, the simulations suggest a mechanistic pathway for the formation of anisotropic clusters from isotropic particles when the lengths of the DNA chains are comparable to the NP size. In this case, at low salt conditions, when the hybridization can already occur, the DNA can fold over the NP to reach the neighboring particle to maximize the number of DNA connections within a bond. If about half of the DNA chains on the particle can participate in the bond then each particle connects with the two nearest complementary NPs. We note that some number of DNAs (out of about 50 per NP) can still be remaining unhybridized due to difficulty in hybridization in such molecularly crowded environment. Hence, at low salt, NP clusters grow linearly with occasional branching when those

dx.doi.org/10.1021/ja501749b | J. Am. Chem. Soc. 2014, 136, 8323−8332

unhybridized DNA are able to form a bond. At higher salt, the persistence length of DNA chains decreases, which results in the reduction of the corona (as shown by our experiments discussed above) and chain rearrangements. It is important to point out that the studied systems are always below the melting temperature of DNA hybridization (Figure S6); therefore, the bonds can be considered irreversible. The free surface area, due to the reduced DNA corona size, allows for adsorption of new particles from the subphase to the interface, and, as shown by X-ray scattering, the NPs remain as monolayer at the interface for all conditions studied.

We propose that hybridization between the newly adsorbed NPs and NPs at the interface occurs via formation of new bonds with those unhybridized DNAs that were not able to bind at low salt conditions. Indeed, the reduced persistence length and softer corona allow for molecular rearrangements which permit reaching the energetically more favorable state of satisfied DNA bonds. The proposed mechanism will contribute to a larger number of local interparticle hybridizations that effectively increases particle "valence" from 0 to 2, 3, and higher. Correspondingly, such connectivity change results (Figure 7) in the transition from an ordered HCP assembly to string-like clusters and, finally, to the large-scale network.[43,44] The lipid interface allows for 2D realization of this pathway. The peculiar feature of the studied 2D system is its crystalline phase (HCP) with a liquid-like rheological response and a disordered state exhibiting elastic behavior. The detailed modeling on DNA chains on the NP and their interactions with each other and a lipid layer at realistic salt conditions is required for the comprehensive understanding of the observed 2D transformations of DNA-coated NPs.

CONCLUSION

By controlling interparticle interactions at an aqueous interface from being purely repulsive to predominantly attractive, we have demonstrated a phase transition from a hexagonally ordered assembly of NPs to a string-like cluster morphology, and finally to a percolating network. This transition is accompanied by significant change in the mechanical behavior of the interface. The rheological properties of the NP layer change from being viscous, to viscoelastic, and to elastic, depending on the 2D assembly morphology and interaction of the NP monolayer with the lipid interface. Our simulations show that the mechanism for the phase transition from the 2D ordered assembly to the string phase cannot be explained simply by the interplay of pairwise interactions. The collective behavior of DNA chains under 2D confinement and their flexibility play crucial roles in inducing this transition. The demonstrated methodology for the assembly of 2D DNA-programmable systems at liquid interfaces opens the possibility for the creation of NP membranes with regulated network topology and mechanical properties, and for the direct testing of predictions of network elasticity for nanoscale systems.[45]

MATERIALS AND METHODS

The charged interfaces were prepared by depositing a monolayer composed of cationic and neutral (zwitterionic) lipids at a water surface by the Langmuir technique.[25] The neutral 1,2-dimyristoyl-*sn*-glycero-3-phosphocholine (DMPC) and cationic lipids, 1,2-dimyristoyl-3-trimethylammonium-propane (DMTAP) were purchased from Avanti Polar Lipids, Inc. The sizes of the gold NPs (solution purchased from Ted Pella) were estimated as 8.5 ± 0.75 nm from SAXS measurements. Gold NPs were functionalized with 50 bases ssDNA using a protocol described elsewhere (SI).[18] The in situ structural evolution due to the change of interparticle and particle–surface interactions are monitored by synchrotron surface scattering techniques. The scattering setup (X22B beamline at the National Synchrotron Light Source) provides simultaneous GISAXS and XRR measurements, which correspondingly probe in-plane and surface-normal monolayer structure. The dynamic interfacial properties were measured using Double Wall Ring (DHR-3 rheometer, TA Instruments) with nano-torque sensitivity. All rheological measurements were performed in the linear regime of the response function tested under amplitude sweep measurements at a fixed oscillatory frequency of 1 Hz. The optimal strains of 2% were used to characterize in situ change of the elastic moduli with the salt-induced structural evolution of the NP monolayer.

ASSOCIATED CONTENT

Supporting Information

Additional experimental details, SAXS modeling, simulation methodology, GISAXS, and XRR. This material is available free of charge via the Internet at http://pubs.acs.org.

AUTHOR INFORMATION

Corresponding Author

ogang@bnl.gov

Notes

The authors declare no competing financial interest.

ACKNOWLEDGMENTS

We thank Prof. G. G. Fuller, Department of Chemistry, Stanford University, for help with interface rheological measurements. Research carried out at the Center for Functional Nanomaterials, Brookhaven National Laboratory, which is supported by the U.S. Department of Energy, Office of Basic Energy Sciences, under Contract No. DE-AC02-98CH10886. M.F. acknowledges support by the U.S. Department of Energy, Office of Basic Energy Sciences, Division of Materials Sciences and Engineering, under Contract No. DE-AC02-98CH10886. Use of the National Synchrotron Light Source was supported by the U.S. Department of Energy, Office of Basic Energy Sciences, under Contract No. DE-AC02-98CH10886.

REFERENCES

(1) Fukuto, M.; Gang, O.; Alvine, K. J.; Ocko, B. M.; Pershan, P. S. *Phys. Rev. E* **2008**, *77*, 031607.
(2) Pershan, P. S.; Braslau, A.; Weiss, A. H.; Alsnielsen, J. *Phys. Rev. A* **1987**, *35*, 4800.
(3) Gang, O.; Ocko, B. M.; Wu, X. Z.; Sirota, E. B.; Deutsch, M. *Phys. Rev. Lett.* **1998**, *80*, 1264.
(4) Ocko, B. M.; Wu, X. Z.; Sirota, E. B.; Sinha, S. K.; Gang, O.; Deutsch, M. *Phys. Rev. E* **1997**, *55*, 3164.
(5) Pontoni, D.; Alvine, K. J.; Checco, A.; Gang, O.; Ocko, B. M.; Pershan, P. S. *Phys. Rev. Lett.* **2009**, *102*, 016101.
(6) Larson, K.; Vaknin, D.; Villavicencio, O.; McGrath, D.; Tsukruk, V. V. *J. Phys. Chem. B* **2002**, *106*, 7246.
(7) Tikhonov, A. M.; Patel, H.; Garde, S.; Schlossman, M. L. *J. Phys. Chem. B* **2006**, *110*, 19093.
(8) Kaganer, V. M.; Mohwald, H.; Dutta, P. *Rev. Mod. Phys.* **1999**, *71*, 779.
(9) Simons, K.; Vaz, W. L. C. *Annu. Rev. Biophys. Biomol. Struct.* **2004**, *33*, 269.
(10) Sanyal, M. K.; Agrawal, V. V.; Bera, M. K.; Kalyanikutty, K. P.; Daillant, J.; Blot, C.; Kubowicz, S.; Konovalov, O.; Rao, C. N. R. *J. Phys. Chem. C* **2008**, *112*, 1739.
(11) Luzinov, I.; Minko, S.; Tsukruk, V. V. *Prog. Polym. Sci.* **2004**, *29*, 635.

(12) Chien, M.-P.; Rush, A. M.; Thompson, M. P.; Gianneschi, N. C. *Angew. Chem., Int. Ed.* **2010**, *49*, 5076.
(13) Cui, M.; Emrick, T.; Russell, T. P. *Science* **2013**, *342*, 460.
(14) Lin, Y.; Skaff, H.; Emrick, T.; Dinsmore, A. D.; Russell, T. P. *Science* **2003**, *299*, 226.
(15) Lin, Y.; Boker, A.; Skaff, H.; Cookson, D.; Dinsmore, A. D.; Emrick, T.; Russell, T. P. *Langmuir* **2005**, *21*, 191.
(16) He, J. B.; Kanjanaboos, P.; Frazer, N. L.; Weis, A.; Lin, X. M.; Jaeger, H. M. *Small* **2010**, *6*, 1449.
(17) He, J. B.; Lin, X. M.; Chan, H.; Vukovic, L.; Kral, P.; Jaeger, H. M. *Nano Lett.* **2011**, *11*, 2430.
(18) Nykypanchuk, D.; Maye, M. M.; van der Lelie, D.; Gang, O. *Nature* **2008**, *451*, 549.
(19) Park, S. Y.; Lytton-Jean, A. K. R.; Lee, B.; Weigand, S.; Schatz, G. C.; Mirkin, C. A. *Nature* **2008**, *451*, 553.
(20) Zhang, Y. G.; Lu, F.; Yager, K. G.; van der Lelie, D.; Gang, O. *Nat. Nanotechnol* **2013**, *8*, 865.
(21) Zhang, C.; Macfarlane, R. J.; Young, K. L.; Choi, C. H. J.; Hao, L.; Auyeung, E.; Liu, G.; Zhou, X.; Mirkin, C. A. *Nat. Mater.* **2013**, *12*, 741.
(22) Geerts, N.; Eiser, E. *Soft Matter* **2010**, *6*, 664.
(23) Senesi, A. J.; Eichelsdoerfer, D. J.; Macfarlane, R. J.; Jones, M. R.; Auyeung, E.; Lee, B.; Mirkin, C. A. *Angew. Chem., Int. Ed.* **2013**, *52*, 6624.
(24) Vial, S.; Nykypanchuk, D.; Yager, K. G.; Tkachenko, A. V.; Gang, O. *ACS Nano* **2013**, *7*, 5437.
(25) Kewalramani, S.; Wang, S. T.; Lin, Y. A.; Huong, G. N.; Wang, Q. A.; Fukuto, M.; Yang, L. *Soft Matter* **2011**, *7*, 939.
(26) Loverde, S. M.; Solis, F. J.; de la Cruz, M. O. *Phys. Rev. Lett.* **2007**, *98*, 237802.
(27) Campolongo, M. J.; Tan, S. J.; Smilgies, D. M.; Zhao, M.; Chen, Y.; Xhangolli, I.; Cheng, W. L.; Luo, D. *ACS Nano* **2011**, *5*, 7978.
(28) Atkins, P.; de Paula, J. *Atkins' Physical Chemistry*, 7th ed.; Oxford University Press: Oxford, 2002.
(29) Parratt, L. G. *Phys. Rev.* **1954**, *95*, 359.
(30) Nelson, A. *J. Appl. Crystallogr.* **2006**, *39*, 273.
(31) Brooks, C. F.; Fuller, G. G.; Frank, C. W.; Robertson, C. R. *Langmuir* **1999**, *15*, 2450.
(32) Srivastava, S.; Nykypanchuk, D.; Maye, M. M.; Tkachenko, A. V.; Gang, O. *Soft Matter* **2013**, *9*, 10452.
(33) Archer, A. J. *Phys. Rev. E* **2008**, *78*, 031402.
(34) Stoycheva, A. D.; Singer, S. J. *Phys. Rev. Lett.* **2000**, *84*, 4657.
(35) Ghezzi, F.; Earnshaw, J. C. *J. Phys.: Condens. Matter* **1997**, *9*, L517.
(36) Seul, M.; Andelman, D. *Science* **1995**, *267*, 476.
(37) Sear, R. P.; Chung, S. W.; Markovich, G.; Gelbart, W. M.; Heath, J. R. *Phys. Rev. E* **1999**, *59*, R6255.
(38) Kwon, H. Y.; Hong, S. S.; Bu, K. M.; Jung, H. S.; Won, C. *J. Korean Phys. Soc.* **2011**, *59*, 75.
(39) Malescio, G.; Pellicane, G. *Phys. Rev. E* **2004**, *70*, 021202.
(40) Frenkel, D.; Smit, B. *Understanding Molecular Simulation: From Algorithms to Applications*, 2nd ed.; Academic Press: San Diego, 2001.
(41) Chi, C.; Vargas-Lara, F.; Tkachenko, A. V.; Starr, F. W.; Gang, O. *ACS Nano* **2012**, *6*, 6793.
(42) Tinland, B.; Pluen, A.; Sturm, J.; Weill, G. *Macromolecules* **1997**, *30*, 5763.
(43) Biffi, S.; Cerbino, R.; Bomboi, F.; Paraboschi, E. M.; Asselta, R.; Sciortino, F.; Bellini, T. *Proc. Natl. Acad. Sci. U.S.A.* **2013**, *110*, 15633.
(44) Romano, F.; Sanz, E.; Tartaglia, P.; Sciortino, F. *J. Phys.: Condens. Matter* **2012**, *24*, 064113.
(45) Sheinman, M.; Broedersz, C. P.; MacKintosh, F. C. *Phys. Rev. E* **2012**, *85*, 021801.